2018 IEEE 15th International Conference on Mobile Ad-hoc and Sensor Systems

Multi-Person Sleeping Respiration Monitoring with COTS WiFi Devices

(Invited Paper)

Yanni Yang*, Jiannong Cao*, Xuefeng Liu†, Kai Xing‡
*The Hong Kong Polytechnic University, Hong Kong, China.
Email: csynyang@comp.polyu.edu.hk, csjcao@comp.polyu.edu.hk
†Beihang University, Beijing, China. Email: csxfliu@gmail.com
‡University of Science and Technology of China, Hefei, China. Email: kxing@ustc.edu.cn

***Abstract*—Recently, non-intrusive respiration monitoring has attracted much attention. Many respiration monitoring systems using the commercial off-the-shelf WiFi devices have been developed. However, these systems mainly have difficulties in the presence of multiple persons. The difficulty generally comes from the separation of the effects of multiple persons' respiration on the received WiFi signals. Another problem is that even though the separation can be feasible with some complicated algorithms, it is still impossible to map the multiple identified respiration states to the corresponding persons. In this paper, we study the problem of multi-person sleeping respiration monitoring and try to address the above challenges. Instead of focusing on developing complicated signal processing algorithms, we take another approach: via the deployment of WiFi transceivers. The key insight comes from the WiFi Fresnel zone model, which indicates that a carefully placed WiFi transceiver may only be affected by the person in a certain location. Furthermore, we consider the sleeping movements of people as well as the sleeping posture change to improve the robustness of the system. Extensive experiments show that we can successfully estimate the respiration rate of multiple persons, with the Mean Absolute Error (MAE) of $0.5\ bpm - 1\ bpm$.**

***Index Terms*—Respiration monitoring; Multi-person scenario; WiFi Fresnel zone.**

I. Introduction

Recently, non-intrusive respiration monitoring, particularly those based on the commercial off-the-shelf (COTS) WiFi devices [1]–[3], attracts much attention. These systems leverage features extracted from the Channel State Information (CSI) of WiFi signals, and from which to infer important information like the respiration rate and the presence of apnea [2], [4].

However, most existing work on WiFi-based respiration monitoring only works for the single-person scenario and have difficulties in the presence of multiple persons. One major difficulty of tracking multiple persons' respiration states comes from the fact that, the chest movement of multiple persons will have accumulative effects on the received WiFi signals that cannot be easily de-coupled. There are many well-designed and complicated algorithms proposed to separate multiple persons' respiration [5]–[7]. However, these methods generally rely on the assumption that the respiration rates of multiple persons are different from each other. Most importantly, existing work for multi-person respiration monitoring is unable to map the identified respiration states to the corresponding persons, which is however of vital importance for performing targeted health analysis for each person exclusively.

In our work, the above problem is addressed through a new perspective: via the deployment of WiFi transceivers. The idea comes from the Fresnel zone model. In [8], [9], the Fresnel zone model is proposed with regards to respiration monitoring. According to the Fresnel zone model, a person at different locations can have different levels of amplitude change for the respiration pattern on the received WiFi signal. Therefore, to capture clear and obvious respiration pattern, the deployment of WiFi transceivers needs to be finely tuned so that the person is located at the good location in the Fresnel zones.

The basic idea of our approach comes from the observation that, under certain deployment of WiFi transceivers, the received WiFi signals can show notable respiration pattern at some locations in the Fresnel zones. While, at some other locations, the respiration pattern can be quite obscure. Delighted by this, we can optimize the deployment of WiFi transceivers, so that each person is only at the good location of a specific transceiver pair, meanwhile at the bad location of all the other transceiver pairs. In this way, we can assign the multi-person respiration monitoring task to multiple transceiver pairs and map the identified respiration state of each transceiver pair to the corresponding person.

However, there are many challenges when realizing the above idea in practice. First, the deployment of WiFi transceivers may lose its effectiveness when people move around and change posture while sleeping, as the respiration pattern is sensitive to the person's location. To ensure decent performance, the deployment of transceiver antennas should still work properly when the person moves. Second, although the effects of other persons' respiration on the target person's received signals can be decreased to the least under the optimized deployment of transceivers, it still cannot be removed completely. However, the minor effects of other persons' respiration can lead to the misinterpretation on the apnea detection for the target person who stops breathing.

To make the deployment more robust when the person moves, the movement of the person on the bed during sleeping is configured to comply with Gaussian distribution. Mean-

2155-6814/18/$31.00 ©2018 IEEE
DOI 10.1109/MASS.2018.00017

while, when the person changes sleeping postures, there would be a vertical displacement change l to the location. So, we combine the Gaussian movement model and vertical change into the optimization process to find the optimal deployment of the transceivers, so that even if the person moves around or changes posture, each transceiver pair can still work properly. In order to precisely detect the presence of apnea, we leverage the observation that the received CSI measurements of the person who stops breathing are quite disordered across different subcarriers compared with that of the person who keeps breathing. Thus, we employ the difference between the maximum and minimum value and the variation of the peak amplitude extracted from the frequency domain among the CSI streams of all the subcarriers to detect the apnea.

To verify the performance of the proposed approach, we implement the system with COTS WiFi devices and evaluate it with extensive experiments which test the precision for the respiration rate estimation and apnea detection.

The main contributions of our work are: (1) Guided by the Fresnel zone model, we find that it is possible to decouple the respiration of multiple persons by carefully deploying the WiFi transceivers. As as result, we can not only monitor multiple persons' respiration simultaneously, but also map the respiration states to the corresponding persons with the specific transceiver pairs, which has not been addressed by previous work. (2) To improve the proposed method in terms of the movement during sleeping and the change of postures, we configure the movement into a Gaussian model and convert the posture change into a vertical displacement to optimize the deployment of transceivers. Furthermore, we draw on the observation of disordered patterns in the received signals to detect the presence of apnea. (3) Through extensive experiments, the multi-person respiration monitoring system can estimate the respiration rate with the Mean Absolute Error of 0.5 bpm - 1 bpm, and the percentage of missed alarm and false alarm for apnea detection is around 8.2% and 7.8% respectively.

II. System Overview

The respiration monitoring system is implemented with COTS WiFi devices. The sketch of the system, with an example of two-person scenario, is shown in Fig. 1. Two persons are lying on the same plane, breathing with different respiration rates. We employ one transmitting (*Tx*) and two receiving antennas (Rx_1 and Rx_2), forming two pairs of transceiver antennas (*Tx*-Rx_1 and *Tx*-Rx_2). Each transceiver antennas pair creates a series of concentric Fresnel zones. The dashed lines in Fig. 1 refer to the boundaries of the Fresnel zones.

The key insight of our system is to leverage the fact that the chest movement of breathing can cause different levels of amplitude change on the received WiFi signals at different locations in the Fresnel zones. The observed respiration pattern from the CSI measurements can be stronger and more obvious for the person who is located in the middle of the Fresnel zones, whereas for the person who is on the boundary of the Fresnel zones, the respiration pattern can be weaker and more obscure. Thereby, we deploy the WiFi transceiver antennas at the specific positions such that each person's respiration only dominates the signals received from a specific receiver.

For the deployment in Fig. 1, the person P_1 is in the middle of the Fresnel zones formed by *Tx*-Rx_1, and also on the boundary of the zones for *Tx*-Rx_2. Inversely, P_2 is in the middle of the Fresnel zones created by *Tx*-Rx_2 while on the boundary of the zones for *Tx*-Rx_1. In this way, there would be more clear respiration pattern for P_1 on the received CSI of Rx_1 than that of P_2. Besides, the signals of Rx_2 show stronger pattern for P_2 than P_1. We can see from Fig. 1, the received signals of Rx_1 and Rx_2 mainly reveal the respiration patterns for P_1 and P_2, respectively. So, we can monitor the respiration of each person with the specific receiver separately and map the identified respiration states to the corresponding persons, *i.e.*, map the state of *Tx*-Rx_1 to P_1 and *Tx*-Rx_2 to P_2.

III. Preliminaries on Respiration Monitoring with WiFi signals

In this section, preliminaries of the respiration effects on WiFi signals is given with respect to the Fresnel zone model, and the effects of different locations in the Fresnel zones on respiration monitoring are discussed.

A. Effects of Respiration on WiFi Signals

During respiration, the chest movement can induce Δd displacement in the anteroposterior and mediolateral dimension of the human body. Δd can vary from $2mm$ to $14mm$ [10], [11]. When the person lies on the back, signals are affected by the anteroposterior change of chest. If the person lies on the side, the change of mediolateral dimension will influence the signals. While breathing, apart from the signals of dynamic paths reflected by the human body, there are also static paths of signals, including the direct signals and those reflected by the stationary objects. Thus, the overall received signals is a combination of the direct and reflected signals.

To characterize the propagation of wireless signals during respiration, the CSI is leveraged. Denote $H(f,t)$ as the CSI measurement for the subcarrier with carrier frequency f at time t. For the indoor environment with static and moving objects, $H(f,t)$ can be expressed as $H(f,t) = H_s(f,t) + H_d(f,t)$. The static vector $H_s(f,t)$ involves the signals of static paths, and the dynamic vector $H_d(f,t)$ contains the reflected signals of the moving object. The amplitude of $H(f,t)$ can be derived as [8]:

$$|H(f,t,\theta)|^2 = |H_s(f,t)|^2 + |H_d(f,t)|^2 + 2\,|H_s(f,t)|\,|H_d(f,t)|\,cos\theta, \tag{1}$$

θ is the phase difference between the vector $H_s(f,t)$ and $H_d(f,t)$. Since the respiration only causes minute change of the signals path, $|H_s(f,t)|$ and $|H_d(f,t)|$ remain almost the same. So, $|H(f,t,\theta)|$ is only affected by the $cos\theta$ term.

B. WiFi Fresnel Zone Model

In indoor environment, wireless signals travelling between the transmitter and receiver can experience the direct path and reflected paths. Fresnel zone is presented to show the effects of

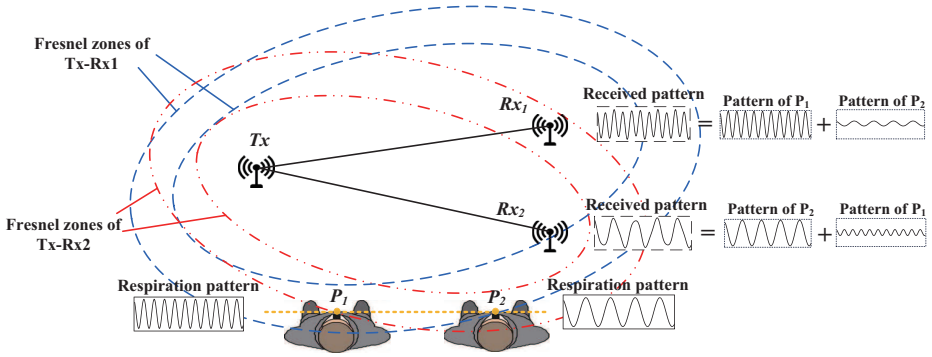

Fig. 1. Sketch of the multi-person sleep respiration monitoring system

the reflected signals on the overall received signals [12]. The Fresnel zones are formed by a series of concentric ellipses with the transmitting and receiving antennas acting as the foci. The boundaries of the Fresnel zones are formulated as:

$$|TP_n| + |RP_n| - |TR| = n \cdot \frac{\lambda}{2} \tag{2}$$

T and R are the transmitting and receiving antennas, λ is the wavelength, and n is the number of the Fresnel zones. An example of the Fresnel zones is depicted in Fig. 1. The dashed ellipses are the boundaries of the Fresnel zones. In [8], [9], the existence of the WiFi Fresnel zones has been verified via elaborate theoretical analysis and experiments.

The boundaries of the Fresnel zones are the places where the reflected signals and direct signal are in-phase or out-of-phase with each other. Hence, if the chest movement travels between the Fresnel zones, there will be periodic increasing and decreasing patterns in the received CSI amplitude.

C. Respiration at Different Locations in the Fresnel Zones

The chest displacement (Δd) while breathing can induce about $2\Delta d$ change of the signal propagation path. Thus, the phase difference $\Delta\theta$ resulting from the chest movement during respiration can be derived as $\Delta\theta \approx 2\pi \cdot \frac{2\Delta d}{\lambda}$. Assume that $\Delta d = 10mm$ and $\lambda = 12cm$ (for $2.4GHz$ WiFi), then the $\Delta\theta$ is $\pi/3$. To investigate the respiration pattern at different locations in the Fresnel zones, we consider the phase difference covers the range of $[-\pi/6, \pi/6]$ or $[\pi/6, 5\pi/6]$. If the person is located at the boundary of the Fresnel zones, then the θ in Eq. (1) is 0. If the person is in the middle of the Fresnel zones, then $\theta = \pi/2$. As shown in Fig. 2, if $\theta = 0$ and the phase difference changes between $[-\pi/6, \pi/6]$, the magnitude of A_1 is quite small. While for $\theta = \pi/2$, with the phase difference covers $[\pi/6, 5\pi/6]$, there can be a notable waveform ($A_2 \gg A_1$). This shows that the received signals show different levels of the amplitude for the respiration pattern at different locations in the Fresnel zones.

Therefore, in order to obtain more obvious respiration pattern with the received CSI measurements, the person is supposed to be in the middle of the Fresnel zones. That is, the

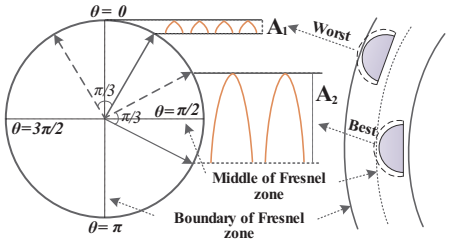

Fig. 2. Received signal at different locations of Fresnel zones

locations of the transmitting antenna (T), receiving antenna (R) and the person (P) should meet the following equation:

$$|TP| + |RP| - |TR| = \frac{2n+1}{4}\lambda \tag{3}$$

While when the person is on the boundary of the Fresnel zones, following Eq. (2), the received signals are more likely to show an unclear respiration pattern.

To give an intuitive presentation, we place the transceiver antennas accordingly to make the person located in the middle and the boundary of the Fresnel zones, respectively. Then, we measure the CSI while the person is breathing. We depict the denoised CSI measurements of all the 30 subcarriers when the person is in the middle (Fig. 3(a)) and on the boundary (Fig. 3(b)) of the Fresnel zones. It shows that, when the person is in the middle of the Fresnel zone, all the CSI streams exhibit notable respiration pattern. While the CSI streams are obscure to show the periodic pattern when the person is on the boundary of the Fresnel zones. This means that the positions of the WiFi transceivers need to be finely adjusted to make the target person located in the middle of the Fresnel zone, so that the observed pattern is clear enough for respiration monitoring. In our work, we leverage this observation to make it as a solution for multi-person sleeping respiration monitoring.

IV. Respiration Monitoring for Multi-person Scenario

In this section, we first demonstrate the realization of multi-person sleeping respiration monitoring by optimizing the deployment of WiFi transceiver antennas. Afterwards, we

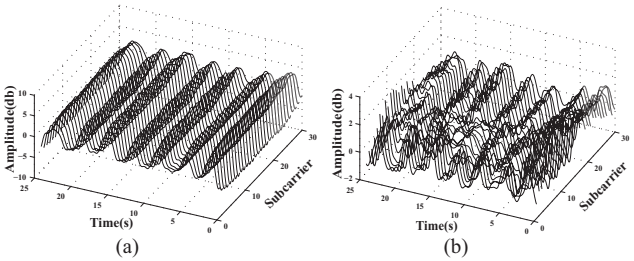

Fig. 3. CSI measurements when the person is (a) in the middle of the Fresnel zone (b) at the boundary of the Fresnel zone

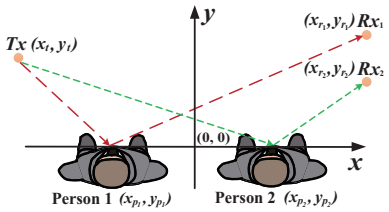

Fig. 4. Lateral view of multi-person respiration monitoring system

perform respiration rate estimation and apnea detection to obtain the respiration states for multiple persons.

A. Optimization of the Deployment of Transceivers

To realize sleep respiration monitoring for multi-person scenario, we need to find the optimal deployment of the transceiver antennas. In this part, we first start from a simple case, where people are fixed at the specific locations and then take the sleeping movement and posture change into account for optimizing the positions of the transceiver antennas.

1) Optimal Positions of Transceiver Antennas for Fixed Locations of Multiple Persons: For the multi-person scenario, suppose we have 1 transmitting antenna, *n* receiving antennas, and *n* concerned persons accordingly. The lateral view of the system setting is depicted in Fig. 4. The target persons and the transceiver antennas are displaced in the same plane for the simplicity of deployment. The original point is the center of the multiple persons. To leverage each pair of transceivers for monitoring multiple persons' respiration separately, we need to set the positions of the transceivers according to Eqs. (2) and (3). For the person P_s, only the antenna pair *Tx*-Rx_s can show notable respiration patterns, while other pairs cannot. Then the positions of transmitting antennas (*Tx*) and receiving antennas (Rx_i) should meet the following equations, where *T* and R_i denote *Tx* and Rx_i:

$$\begin{aligned} |TP_s| + |R_iP_s| - |TR_i| &= \frac{(2n_s^i + 1)\cdot\lambda}{4}, i = s \\ |TP_s| + |R_iP_s| - |TR_i| &= \frac{n_s^i \cdot \lambda}{2}, i \neq s \end{aligned} \tag{4}$$

However, the above equations may not be satisfied at the same time. Therefore, we transform it into an optimization problem, which is to find the optimal positions of the transceiver antennas according to the fixed and known locations of multiple persons. The objective is to maximize the amplitude of the received CSI for *Tx*-Rx_s for the person P_s and minimize the amplitude of the received CSI for *Tx*-Rx_i, where $i \neq s$. This means that, with phase difference $|\theta_s - \theta_{s'}|$, the amplitude of $|cos(\theta_s) - cos(\theta_{s'})|$ should be maximized for the person P_s of *Tx*-Rx_s, and minimized for *Tx*-Rx_i when $i \neq s$. θ_s and $\theta_{s'}$ are the phase values when the person does not breathe and breathes to the highest magnitude respectively, derived as:

$$\theta_{s,i} = \frac{2\pi}{\lambda}(|TP_s| + |R_iP_s| - |TR_i|) \tag{5}$$

Then, the objective function $F(s,i)$ can be formulated as:

$$\begin{aligned} \max_{Rx_i} F(s,i) &= \sum_{s,i=1}^{n,n} f(s,i), \\ f(s,i) &= \frac{|cos(\theta_{s',s}) - cos(\theta_{s',s})|}{\sum_{i\neq s}^{n} |cos(\theta_{s,i}) - cos(\theta_{s',i})|} \end{aligned} \tag{6}$$

We test the above optimization process with the initial settings in Table I and Table II for two-person and three-person scenarios. For the simplicity of the system deployment, the T_x is fixed and the receivers are traversed along the x-axis with a step of $0.02m$. We plot all the values of the objective function for the two-person and three-person scenarios in Fig. 5(a) and Fig. 5(b). Then, we retrieve the positions of receivers of which the objective function reaches the maximum. In this example, for the two-person scenario, Rx_1 and Rx_2 are placed to $(1.32m, 0.8m)$ and $(1.38m, 0.6m)$. While for the three-person scenario, Rx_1, Rx_2 and Rx_3 are obtained as $(1.28m, 1m)$, $(1.42m, 0.8m)$ and $(1.14m, 0.6m)$. The computation time of the optimization process for the two-person and three-person scenarios is $0.53s$ and $16.7s$ respectively.

2) Optimal Positions of Transceiver Antennas with Human Movement and Posture Change: In practice, it is not enough to settle down the optimal positions of *Tx* and *Rx* with only fixed locations of the concerned persons, since the person will move around and change posture in the sleeping area. Empirically, people tend to move to the points closer to the fixed location with higher probability and it is less likely for them to move far away. So the movement model P_s is configured to comply with the Gaussian distribution as follows:

$$\begin{aligned} P_s &\sim N(\mu, \sigma^2), \\ g(x) &= \frac{1}{\sqrt{2\pi}\sigma} exp(-\frac{(x-\mu)^2}{2\sigma^2}) \end{aligned} \tag{7}$$

TABLE I
INITIAL SETTINGS FOR TWO-PERSON SCENARIO

T_x, Δd	(-1m, 1m), 0.08m
P_1, P_2	(-0.3m, 0m), (0.3m, 0m)
R_1, R_2	$(1m, 0.8m) \sim (2.5m, 0.8m)$, $(1m, 0.6m) \sim (2.5m, 0.6m)$

TABLE II
INITIAL SETTINGS FOR THREE-PERSON SCENARIO

T_x, Δd	(-1.3m, 1m), 0.08m
P_1, P_2, P_3	(-0.5m, 0m), (0m, 0m), (0.5m, 0m)
R_1, R_2, R_3	$(1m, 1m) \sim (2.5m, 1m)$, $(1m, 0.8m) \sim (2.5m, 0.8m)$, $(1m, 0.6m) \sim (2.5m, 0.6m)$

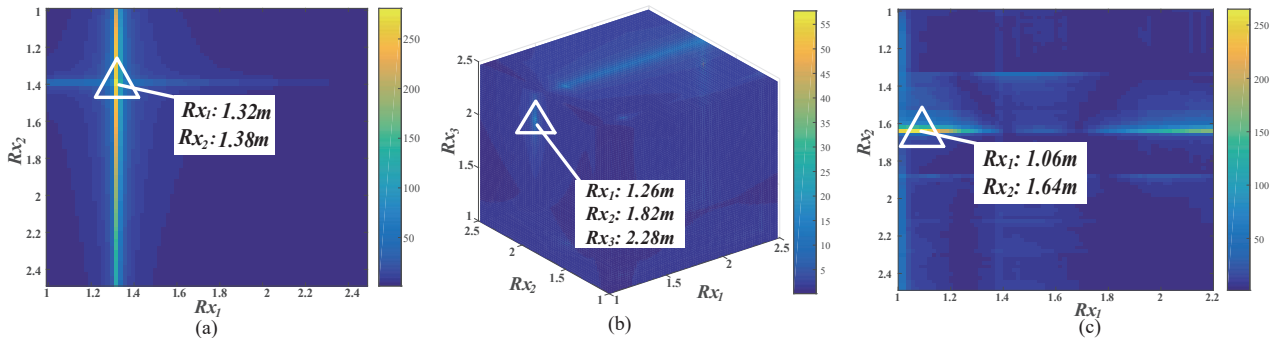

Fig. 5. Optimal positions of receivers for (a) fixed locations of two persons (b) fixed locations of three persons (c) dynamic locations of two persons.

$g(x)$ is the probability density function of the movement model regarding the moving distance x. In addition, there are cases when people change sleeping posture. The common sleeping postures can be classified into two categories: one includes the Starfish, Soldier and Freefaller, which belong to the posture of lying on the back; the other consists of the Log, Foetus and Yearner, regarded as lying on the side [13]. Changing from the above two kinds of postures, there will be a vertical displacement change l for the person's location. Thus, we also need to consider the presence of l in the optimization process.

To make the deployment more robust in face of the movement and posture change, the Gaussian movement model and vertical change of l are integrated into the objective function. The P_s in Eq. (6) is replaced by $P(g(s))$ to represent the location distribution resulting from the movement for the target person, and the vertical change l is also added, creating the revised objective function as follows:

$$\max_{Rx_i} F(s,i) = \sum_{s,i=1}^{n,n} \int_{-r}^{r} [\frac{1}{2} f(g(s),i) + \frac{1}{2} f(g(s)+l,i)], \quad (8)$$

r is the upper bound of the moving distance. For the Gaussian model, $\mu = 0$ and the effects of variance σ and l will be discussed in the evaluation part. Here, we give an example on the two-person scenario for the above optimization process. The initial setting is the same as Table I, and $\mu = 0$, $\sigma = 0.06$, $l = 0.2m$, $r = 0.2m$. The visualization of the objective function is shown in Fig. 5(c). The positions of Rx_1 and Rx_2 are changed to $(1.06m, 0.8m)$ and $(1.64m, 0.6m)$. The computation time for running the above optimization process is around $460s$, since it takes longer time for the iterated operation of performing integral. The above optimization process for determining the optimal positions of transceiver antennas is performed off-line. It only requires one-time preparation for the deployment of transceivers before respiration monitoring.

B. Respiration State Estimation

In this part, we identify the respiration states, including the respiration rate and the presence of apnea with the CSI measurements via frequency-domain and time-domain analysis.

1) Respiration Rate Estimation: Since raw CSI measurements contain many signal noises, we apply the Hampel [14] and wavelet filter [15] on the CSI series to remove outliers and high-frequency noises. Next, the respiration rate is estimated by performing the Fast Fourier Transformation (FFT) on all the CSI streams. Within the range $[0.1Hz, 0.6Hz]$ of respiration rate, the highest peak of the summation of all the FFT results can refer to the respiration rate of the target person, since each time series shows periodic respiration pattern. However, we find that there is a frequency leakage induced by the default rectangular window added on the CSI stream for the FFT calculation. To eliminate the frequency leakage on respiration rate estimation, we add a hamming window on each CSI stream, and apply the method mentioned in [16] to give a precise estimation on the respiration rate.

We use the above method to estimate the respiration rate under multi-person scenario as shown in Fig. 6. When people breathe with different respiration rates, there are multiple peaks in the FFT results, *e.g.*, the two peaks in Fig. 6(a) and three peaks in Fig. 7 for two-person and three-person scenario. In Fig. 6(a), the highest peak in the FFT result of *Tx-Rx*$_1$ is incurred by the breathing of P_1, as *Tx-Rx*$_1$ is set to monitor P_1's respiration. While the frequency of highest value in *Tx-Rx*$_2$ is the respiration rate of P_2. In this way, we can not only estimate the respiration rate, but also map the identified respiration state of *Tx-Rx*$_1$ to P_1 and that of *Tx-Rx*$_2$ to P_2. Similar observation is also applied to three-person scenario as in Fig. 7. When people are breathing with similar respiration rate, there is only one peak in the FFT results as in Fig. 6(b).

2) Apnea Detection: Intuitively, when multiple persons breathe with different rates, the apnea can be detected by observing the disappearance of the peaks in the FFT results. However, if one person stops breathing, there is still a minor peak value in the FFT result incurred by other persons' respiration, which can result in a false judgement that the person is still breathing. Furthermore, as the variation of the respiration rate while sleeping is only $2.2-3.0$ bpm [17], there will be times when different persons have similar breathing rate. If people have similar respiration rate, apnea can be more difficult to be detected from change of the peak value in the FFT results, as only one major peak is left in the FFT results.

For apnea detection under multi-person scenario, we find that the peak amplitude in the FFT results for the person who stops breathing is smaller than those who are still breathing. For example, Fig. 6(c) shows the FFT results for the two per-

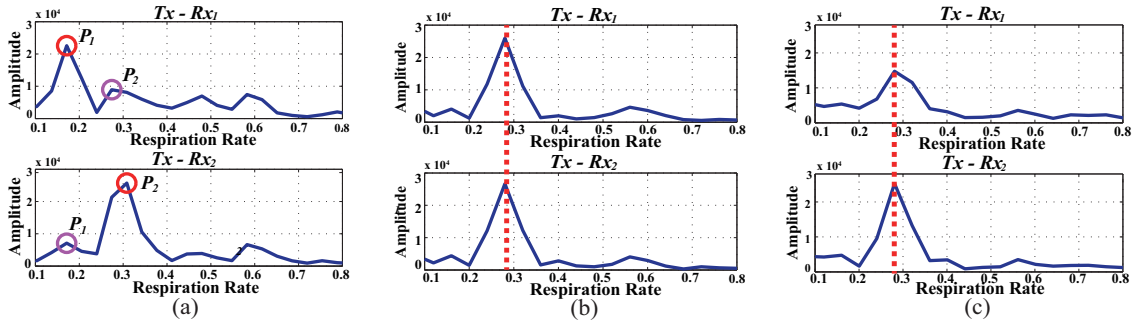

Fig. 6. (a) FFT results for two-person scenario with different respiration rates. (b) FFT results of two-person scenario with similar respiration rates. (c) FFT results of two-person scenario when P_1 stops breathing.

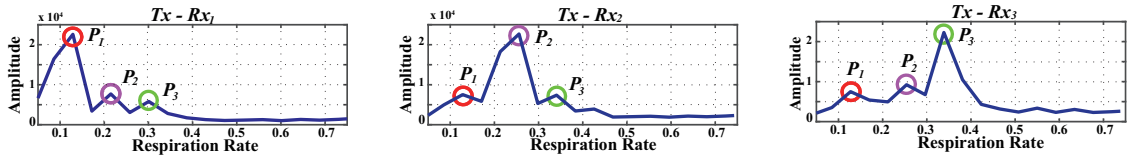

Fig. 7. FFT results for three-person scenario when P_1, P_2 and P_3 have different respiration rates with three pairs of transceivers (Tx-Rx_1,Tx-Rx_2, Tx-Rx_3)

sons with similar respiration rate, in which P_1 stops breathing. However, it is difficult to give a quantitative description of the peak value difference for detecting the apnea. Therefore, we also exploit another observation: when the person stops breathing, the WiFi signals will be affected by other persons who are on the boundary of the Fresnel zones, where the patterns on the CSI measurements are pretty disordered and obscure. This means the amplitude of the highest peak in the FFT results can vary greatly among different subcarriers.

The distribution of the highest peak amplitude for all the subcarriers is illustrated in Fig. 8. It shows that when the person stops breathing, the peak value varies in a larger range than that of the person who keeps breathing. So, we calculate the difference between the maximum and minimum peak amplitude, and the variation of the peak amplitude among subcarriers from the FFT results for each pair of antennas. Then, the following condition is used to detect apnea:

$$
\begin{aligned}
Diff_{i,j} &= \frac{|sum[peak_i(n)] - sum[peak_j(n)]|}{max(sum[peak_i(n)], sum[peak_j(n)])} \\
Dev_{i,j} &= \frac{|var[peak_i(n)] - var[peak_j(n)]|}{max(var[peak_i(n)], var[peak_j(n)])} \\
Diff_{i,j} &+ Dev_{i,j} > \sigma_2
\end{aligned}
\tag{9}
$$

$peak_i(n)$ is the vector of the peak amplitude of all the subcarriers. Once the above term is met, we claim that the person who stops breathing can be settled as the one whose difference and variance of the peak amplitude are above the threshold. σ_2 is empirically set to be 0.8.

V. Evaluation

In this section, the results from the extensive experiments on the respiration rate estimation and apnea detection are given, and the effects of different parameters influencing the system performance are also discussed.

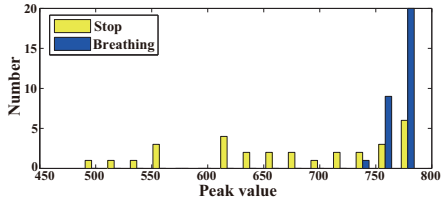

Fig. 8. Histogram distribution of peak amplitude for two persons (P_1 stops breathing, P_2 breathes)

A. Implementation

The system is built with COTS WiFi devices, *i.e.* Intel 5300 NIC and TP-Link WR841N wireless router. The NIC is installed on the Lenovo B460 laptop. CSI measurements are collected with a CSI tool [18] which can be operated on the Ubuntu 12.04 system, and processed using MATLAB 2016a. The wireless router operates on $2.4GHz$ with $20MHz$ bandwidth channels, which is commonly used in people's daily life. An example of the system implementation is shown in Fig. 9. After obtaining the locations of all the concerned persons, the transmitting and receiving antennas can be displayed according to the positions automatically calculated by the optimization process to monitor peoples respiration.

B. Evaluation Metrics

To evaluate the performance of the respiration monitoring system, 5 subjects, including 2 males and 3 females with different figures are recruited during two months to collect the CSI measurements while breathing. While breathing, the ground truth of the respiration state is recorded by the chest strap worn on the subject's body. To evaluate the accuracy of respiration rate estimation, we calculate the Mean Absolute Error (MAE) between the estimated result and the actual

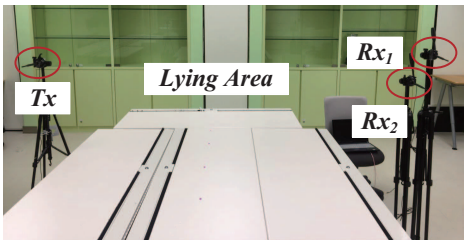

Fig. 9. Illustration of system implementation

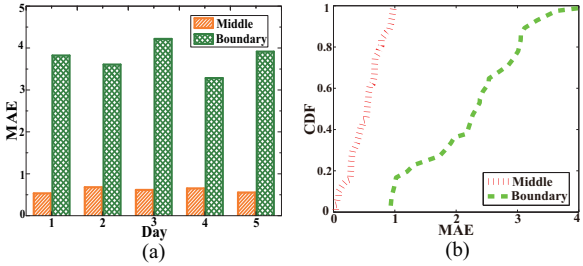

Fig. 10. Effect of different locations. (a) MAE on each day. (b) CDF plot at different locations.

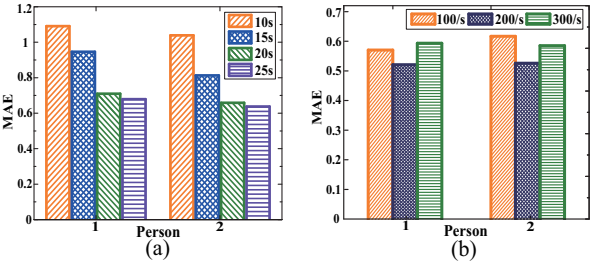

Fig. 11. MAE of (a) different window sizes (b) different sampling rates.

respiration rate. The respiration rate is in the form of bpm (breath per minute).

$$MAE = \frac{\sum_{i=1}^{n} |R_i' - R_i|}{n}, \tag{10}$$

R_i and R_i' correspond to the estimated and the actual respiration rate of the person, respectively.

Then, we carry out experiments on the apnea detection and obtain the percentage of the missed and false alarm for detecting the apnea. The missed alarm (MA) is the percentage of the missed cases of apnea among all the real apnea cases, while the false alarm (FA) is the percentage of the misjudgment of apnea among the samples with no apnea.

C. Respiration Rate Estimation

To verify the performance of the proposed method for respiration rate estimation, we evaluate the accuracy of respiration rate estimation with respect to the effects of different locations, window size, sampling rate, respiration patterns, size of variance σ for the Gaussian model and vertical change l.

1) Effect of different locations in Fresnel zone: First, we investigate the effects of different locations in the Fresnel zones on respiration rate estimation. In Fig. 10, when the subject is in the middle of the Fresnel zones, the average MAE is 0.614 bpm, which means that the error of estimating the respiration rate in a minute does not exceed one breath. We also give results of the respiration rate when the person is on the boundary of the Fresnel zones, of which the mean value is 3.130 bpm. It is around 5 times higher than the MAE when the person is in the middle of the Fresnel zones, indicating worse performance on respiration rate estimation.

2) Effects of window size and sampling rate: Next, we investigate the impact of the window size and sampling rate for estimating respiration rate. Figure. 11(a) shows the MAE with different window sizes. It can be seen that larger window size can achieve a smaller MAE, and the MAE of the window sizes of $20s$ and $25s$ is similar. To increase the realtime performance and ensure the accuracy, we choose the window size of $20s$. While for different sampling rates, $100p/s$, $200p/s$ and $300p/s$ are set for CSI measurements collection. The sampling rate of $200p/s$ is selected because of its higher accuracy due to it higher resolution in frequency domain and smaller noises in the CSI measurements, as shown in Fig. 11(b).

3) Effects of different respiration patterns: The MAE of the estimated respiration rate for different numbers of people with different respiration patterns is shown in Fig. 12(a). The average MAE for the multi-person scenario under different respiration patterns is 0.750 bpm, which is slightly higher than the single-person scenario. The MAE of similar respiration rate is smaller than that of different respiration rates, because similar respiration pattern suffers from less noises. In addition, the MAE of the two-person scenario is slightly lower than that of the three-person scenario, in that the more number of persons involved, the more compromises need to be made for finding the optimal positions of the transceiver antennas.

4) Effects of variance σ in the Gaussian model: The effects of the variance σ in the Gaussian movement model are investigated with the σ change from 0.04 to 0.065 with step of 0.005 for three cases: the person does not move ($L = 0cm$), move $L = 5cm$ and $L = 10cm$ around the fixed position. From Fig. 12(b), it can be seen that the larger distance of the movement, the higher the MAE will be with the loss of deployment effectiveness steadily. Since the probability density function has the highest probability at the fixed location, *i.e.*, the location of the mean value ($\mu = 0$), the MAE of $L = 0cm$ becomes the smallest. Meanwhile, the MAE under movement scenarios reaches the minimum when the variance σ is 0.06.

5) Effects of vertical change of l: To see the effects of the size for the vertical change of l considering the change of two categories of sleeping postures, three persons with different shoulder breadth: $No.1 : 36cm$, $No.2 : 41cm$ $No.3 : 45cm$ are selected. The results on respiration rate estimation under different vertical change l when they change the posture from lying the back to lying on the side is shown in Fig. 12(c). For the person with shorter shoulder breadth, better result can be achieved with smaller l, while larger l brings better results

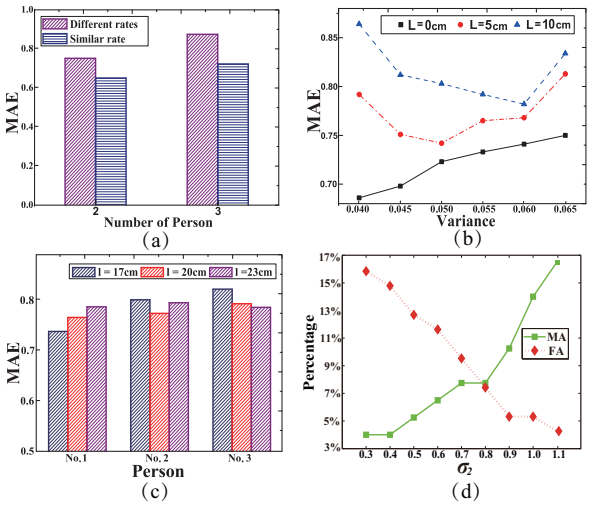

Fig. 12. (a) MAE of different respiration patterns (b) MAE of different σ and L (c) MAE of different l (d) Effects of σ_2 on the apnea detection

for bigger-size person. It also indicates the difference among the MAE results is not too much. Hence, to make it more adaptive for different people, we can take the average value as the vertical change in the optimization process.

D. Apnea Detection

In the multi-person scenario, we evaluate the accuracy of apnea detection from two aspects: (1) the performance of apnea detection under similar and different respiration rates. (2) the performance of apnea detection under moving around and posture change scenarios.

1) Impact of the σ_2: The σ_2, as the threshold to compare the difference and variation of peak amplitude of different CSI streams, can affect the result of apnea detection. Therefore, we adjust σ_2 in the range of $[0.3, 1.1]$ and calculate the (MA) and (FA). The values of MA and FA under different σ_2 are illustrated in Fig. 12(d). It can be seen that the MA increases steadily with the rising of σ_2 while FA is smaller with larger σ_2. Since both MA and FA would be the lower the better, therefore we make the σ_2 to be 0.8 since MA and FA are relatively low at this point with a overall better performance.

TABLE III
RESULTS OF APNEA DETECTION

	MA	FA
Different rates	5.42%	5.17%
Similar rates	8.75%	8.42%
Average	7.09%	6.80%

TABLE IV
RESULTS OF APNEA DETECTION

	MA	FA
Move $5cm$	7.52%	7.61%
Move $10cm$	9.23%	8.54%
Lie on back	6.95%	6.23%
Lie on side	8.74%	8.82%

2) Accuracy of apnea detection: The results of apnea detection with different and similar respiration rates are shown in Table III. The MA and FA for multiple persons who have different respiration rates are both lower than that of similar respiration rates. Although the apnea detection for the persons with similar respiration rates tends to be more difficult, the MA and FA are still at a relatively low level with our method.

The results of apnea detection under moving around and posture change scenarios are shown in Table. IV. The MA and FA increase with the extension of moving distance, and both higher than the average result in Table. III at the fixed location. Furthermore, the performance of apnea detection is better for lying on the back scenario than that of the lying the side scenario. It is because the posture change does not result in the same vertical change in practice, so that the performance cannot reach the expected results.

VI. RELATED WORK

Our work on multi-person respiration monitoring is mostly related to non-intrusive respiration monitoring using wireless signals, summarized as follows.

A. Human Respiration Monitoring with WiFi Signals:

In recent years, with the popularity of WiFi devices, researchers are dedicated to leverage the COTS WiFi devices for device-free respiration monitoring. At first, the RSSI is leveraged [1], [19]–[22] for respiration monitoring, however RSSI is less sensitive to the chest movement, since it only provides coarse-grained information of the WiFi signals. Thus, it requires a densely deployed wireless network to achieve decent results. Comparing with RSSI, CSI can provide more fine-grained information of the wireless links, and it can better detect the minute chest movement from the wireless signals [2]–[4], [8]. In [8], authors introduce the Fresnel zone and lay the general theoretical foundation for human behavior recognition with RF signals, with emphasis on respiration monitoring using WiFi signals, which provides a basic understanding for wireless human sensing.

B. Multi-person Respiration Monitoring via Wireless Signals:

There are many studies into the problem of respiration monitoring with wireless signals. However, only few of the present work deals with the problem of multi-person respiration monitoring using WiFi signals, as listed in Table V. Existing work provides many feasible plans for multi-person respiration monitoring via WiFi signals. Some perform the Power Spectrum Density (PSD) algorithm on the received

TABLE V
COMPARISON OF WORKS IN MULTI-PERSON RESPIRATION MONITORING

Work	Number	Accuracy	Mapping
[3]	2 persons	0.5-1 bpm	No
[8]	2 persons	–	No
[7]	multi-person	0.5-1 bpm	No
[5]	multi-person	0.5-1.2 bpm	No
Our work	multi-person	0.5 - 1 bpm	Yes

WiFi signals to extract the respiration rates of two persons [3], [8]. In [7], Root-MUSIC algorithm is leveraged to obtain the respiration rates of multiple persons. [5] applies tensor decomposition on the phase difference to create a CSI tensor and estimate multiple persons' respiration rates. These methods are based on the assumption that different people have different respiration pattern. Moreover, these approaches cannot map the estimated respiration rates to each of the monitored persons, which is essential to perform respiratory state analysis of each target person. In [16], [23], FMCW radar is applied to separate the signals reflected by different persons based on their reflection time. However, it requires specialized and expensive hardware and cannot give precise estimation if the two persons are too close to each other.

VII. Limitation and Future Work

For respiration monitoring with WiFi signals, the respiration pattern on the received signals has different levels of amplitude change for different locations in the Fresnel zones. Although, this feature brings opportunities for multi-person respiration monitoring, and we can even map the identified respiration states to the corresponding persons, the performance will degrade with the increasing of number of people, as there will be more constraints in the optimization process, making the deployment not well suited for each of the person.

For the future work on multi-person respiration monitoring with WiFi signals, insight can be given to the $60GHz$ millimeter wave WiFi devices, in that the $60GHz$ millimeter wave has shorter wavelength (5mm) [24], which is much smaller than that of the $2.4GHz$ and $5GHz$ WiFi devices. Therefore, while breathing, the chest movement is more like to go through multiple Fresnel zones. However, $60GHz$ millimeter wave has high directionality which also poses challenges and multi-person respiration monitoring and the $60GHz$ WiFi devices are quite expensive currently for wide deployment .

VIII. Conclusion

In this paper, we develop a multi-person sleeping respiration monitoring system with COTS WiFi devices. We try to separate the effects of multiple person's respiration on the received WiFi signals, and map the identified respiration states to individual persons. The key insight of our system comes from the WiFi Fresnel zone model, which indicates that the chest movement of breathing can cause different levels of amplitude change on the received WiFi signals at different locations. Thereby, we manage to find the optimal deployment of the WiFi transceiver antennas with optimization process and take the movement model and sleeping posture change into account. Then, the WiFi transceiver antennas are placed at specific places such that each person's respiration only dominates the signals received from a specific receiver.

Acknowledgment

The work in this paper was supported in part by the NSFC Key Grant with Project No. 61332004 and Hong Kong RGC General Research Fund under Grant PolyU 152244/15E.

References

[1] H. Abdelnasser, K. A. Harras, and M. Youssef, "Ubibreathe: A ubiquitous non-invasive wifi-based breathing estimator," in *MobiHoc, ACM, 2015*.

[2] X. Liu, J. Cao, S. Tang, and J. Wen, "Wi-sleep: Contactless sleep monitoring via wifi signals," in *RTSS, IEEE, 2014*.

[3] J. Liu, Y. Wang, Y. Chen, J. Yang, X. Chen, and J. Cheng, "Tracking vital signs during sleep leveraging off-the-shelf wifi," in *MobicHoc, ACM, 2015*.

[4] X. Liu, J. Cao, S. Tang, J. Wen, and P. Guo, "Contactless Respiration Monitoring Via Off-the-Shelf WiFi Devices," *IEEE Transactions on Mobile Computing*, vol. 15, no. 10, pp. 2466–2479, 2016.

[5] X. Wang, C. Yang, and S. Mao, "TensorBeat: Tensor Decomposition for Monitoring Multi-person Breathing Beats with Commodity WiFi," *ACM Transactions on Intelligent Systems and Technology*, 2017.

[6] C. Chen, Y. Han, Y. Chen, and K. J. R. Liu, "Multi-person Breathing Rate Estimation Using Time-reversal on WiFi Platforms," in *GlobalSIP, IEEE, 2016*.

[7] X. Wang, C. Yang, and S. Mao, "Phasebeat: Exploiting csi phase data for vital sign monitoring with commodity wifi devices," in *ICDCS, IEEE, 2017*.

[8] H. Wang, D. Zhang, J. Ma, Y. Wang, Y. Wang, D. Wu, T. Gu, and B. Xie, "Human respiration detection with commodity wifi devices: do user location and body orientation matter?" in *Ubicomp, ACM, 2016*.

[9] F. Zhang, D. Zhang, J. Xiong, H. Wang, K. Niu, B. Jin, and Y. Wang, "From fresnel diffraction model to fine-grained human respiration sensing with commodity wi-fi devices," *Ubicomp, ACM, 2018*.

[10] A. De Groote, M. Wantier, G. Chéron, M. Estenne, and M. Paiva, "Chest Wall Motion during Tidal Breathing," *Journal of Applied Physiology*, vol. 83, no. 5, pp. 1531–1537, 1997.

[11] G. Shafiq and K. C. Veluvolu, "Surface Chest Motion Decomposition for Cardiovascular Monitoring," *Scientific reports*, vol. 4, 2014.

[12] J. C. Wiltse, "History and Evolution of Fresnel Zone Plate Antennas for Microwaves and Millimeter Waves," in *Antennas and Propagation Society International Symposium, 1999. IEEE*, vol. 2, pp. 722–725.

[13] BBC, "Sleep position gives personality clue," http://news.bbc.co.uk/2/hi/health/3112170.stm/, 2003.

[14] L. Davies and U. Gather, "The identification of multiple outliers," *Journal of the American Statistical Association*, vol. 88, no. 423, pp. 782–792, 1993.

[15] J. D. Villasenor, B. Belzer, and J. Liao, "Wavelet Filter Evaluation for Image Compression," *IEEE Transactions on image processing*, vol. 4, no. 8, pp. 1053–1060, 1995.

[16] F. Adib, H. Mao, Z. Kabelac, D. Katabi, and R. C. Miller, "Smart homes that monitor breathing and heart rate," in *CHI, ACM, 2015*.

[17] G. Gutierrez, J. Williams, G. A. Alrehaili, A. Mclean, R. Pirouz, R. Amdur, V. Jain, J. Ahari, A. Bawa, and S. Kimbro, "Respiratory Rate Variability in Sleeping Adults without Obstructive Sleep Apnea," *Physiological Reports*, vol. 4, no. 17, 2016.

[18] D. Halperin, W. Hu, A. Sheth, and D. Wetherall, "Tool Release: Gathering 802.11n Traces with Channel State Information," *ACM SIGCOMM Computer Communication Review*, vol. 41, no. 1, pp. 53–53, 2011.

[19] N. Patwari, J. Wilson, S. Ananthanarayanan, S. K. Kasera, and D. R. Westenskow, "Monitoring Breathing via Signal Strength in Wireless Networks," *IEEE Transactions on Mobile Computing*, vol. 13, no. 8, pp. 1774–1786, 2014.

[20] N. Patwari, L. Brewer, Q. Tate, O. Kaltiokallio, and M. Bocca, "Breathfinding: A Wireless Network That Monitors and Locates Breathing in a Home," *IEEE Journal of Selected Topics in Signal Processing*, vol. 8, no. 1, pp. 30–42, 2014.

[21] O. J. Kaltiokallio, H. Yigitler, R. Jäntti, and N. Patwari, "Non-invasive respiration rate monitoring using a single cots tx-rx pair," in *IPSN, IEEE, 2014*.

[22] Y. Zhao, J. Ashe, and T. Yu, "Respiration monitoring using a wireless network with space and frequency diversities," in *ICCE, IEEE, 2016*.

[23] M. Zhao, F. Adib, and D. Katabi, "Emotion recognition using wireless signals," in *Mobicom, ACM, 2016*.

[24] B. Bosco, R. Emrick, S. Franson, J. Holmes, and S. Rockwell, "Emerging commercial applications using the 60 ghz unlicensed band: Opportunities and challenges," in *WAMICON, IEEE, 2006*.